SUPPLEMENTARY INFORMATION

Rising Heatwaves and Their Implications for China’s Solar Power and Carbon Neutrality Goals

Xinghong Cheng[1], Daoming Zhu[1], Duanyang Liu[2], Chunsong Lu[3], Xiangde Xu[1], Deliang Chen[4], Yanbo Shen[5], Shuqi Yan[2], Zirui Du[3], Naifu Shao[6], Zhongfeng Xu[7], Bing Chen[8], Wei Duan[9]

[1]State Key Laboratory of Severe Weather Meteorological Science and Technology (LaSW), Chinese Academy of Meteorological Sciences, Beijing 100081, China.
[2]Key Laboratory of Transportation Meteorology of CMA / Jiangsu Key Laboratory of Severe Storm Disaster Risk, Nanjing Innovation Institute for Atmospheric Sciences, Chinese Academy of Meteorological Sciences–Jiangsu Meteorological Service, Nanjing 210041, China.
[3]Nanjing University of Information Science and Technology, Nanjing 210044, China.
[4]Tsinghua University, Beijing 100084, China.
[5]Key Laboratory of Energy Meteorology of CMA / China Meteorological Administration Public Meteorological Service Center, Beijing 100081, China.
[6]Tianjin Climate Center, Tianjin 300074, China.
[7]State Key Laboratory of Earth System Numerical Modeling and Application, Institute of Atmospheric Physics, Chinese Academy of Sciences, Beijing 100029, China.
[8]Institute of Plateau Meteorology, China Meteorological Administration, Chengdu 610213, China.
[9]Yunnan Institute of Meteorology Sciences, Kunming 650034, China.

This file includes:

Supplementary Notes

Supplementary Note 1. Simulation settings

We used the open-source Weather Research and Forecasting model coupled with Chemistry (WRF-Chem, version 4.2.2)[1] to simulate the spatiotemporal variations of surface shortwave solar radiation, air temperature (Ta), total cloud cover (TCC), and aerosol optical depth (AOD) across China during summer at five-year intervals from 2015 to 2060. The model domain covers China and surrounding regions at a horizontal resolution of 10 km × 10 km, with 41 vertical layers of variable thickness extending from the surface to 10 hPa. A double-nested grid configuration was adopted, consisting of outer and inner domains at 50 km and 10 km resolution, respectively (Supplementary Fig. 1), with hourly output frequency.

The simulations were driven by monthly emissions from the Dynamic Projection model for Emissions in China (DPEC, version 1.1)[2] for the carbon-neutral scenario at five-year intervals (0.25° × 0.25° resolution). Meteorological initial and boundary conditions were obtained from a 6-hourly, bias-corrected, multi-model integrated CMIP6 dataset[3], constructed as the ensemble mean of 18 GCMs (1.25° resolution). Chemical initial and boundary conditions were derived from the MOZART-4 global chemical transport model[4]. A summary of all input datasets is provided in Supplementary Table 1.

The following physical parameterization schemes were employed in WRF-Chem: the improved Morrison two-moment microphysics scheme[5], RRTMG longwave and shortwave radiation schemes[6], revised Monin–Obukhov surface layer scheme[7], Grell 3D ensemble cumulus parameterization[8], RUC land surface model[9], and Shin–Hong planetary boundary layer scheme[10]. Parameters used for PV power calculations and associated losses are provided in Supplementary Tables 2 and 3.

Supplementary Note 2. Simulation validation

To evaluate the reliability of simulated global horizontal irradiance (GHI), direct normal irradiance (DNI), diffuse horizontal irradiance (DHI), and air temperature (Ta) for the summers of 2015 and 2020, we compared model outputs with hourly observations from national meteorological stations. The number of stations measuring DNI and DHI is considerably lower than those for GHI, and fewer Ta observations were available in 2015 than in 2020.

We calculated correlation coefficient (R), root-mean-square error (RMSE), mean bias (MB), normalized mean bias (NMB), and index of agreement (IOA) using monthly averaged model outputs and observations for June–August of 2015 and 2020 (Supplementary Table 4).

Correlation coefficients between simulations and observations for GHI, DNI, DHI, and Ta were all above 0.61 and statistically significant at the 99.9% confidence level. IOA values exceeded 0.73 for all variables, indicating strong agreement in the spatiotemporal variability of surface radiation and temperature. The model generally overestimates GHI, DNI, DHI, and Ta, with the largest biases for GHI and DNI. RMSE and MB for DHI and Ta are relatively small (NMB $\approx$ 1%), whereas GHI and DNI exhibit larger errors (NMB up to 16%). These biases likely stem from uncertainties in simulated TCC and AOD, which in turn reflect limitations of the driving GCM and emission inventory.

Supplementary Note 3. Interannual variation of solar radiation, high-temperature days and power loss distribution

To examine the spatiotemporal stability of solar radiation, extreme hot days (EHD), and PV power losses during summer, we evaluated the spatial distributions of GHI, EHD, and PV power loss from 2015 to 2060 at five-year intervals (Supplementary Figs. 2–4).

Throughout the study period, western China—including Xizang (Tibet), Qinghai, Xinjiang, and the western portions of Sichuan, Gansu, and Inner Mongolia—maintained consistently high GHI values with strong spatial persistence. Elevated GHI also appeared in Shanxi

Province and the Beijing–Tianjin–Hebei (BTH) region in 2035, 2040, 2055, and 2060, and in Hunan and Jiangxi in 2015 and 2060, though with lower spatial stability. In contrast, southeastern Tibet, central and eastern Sichuan, Northeast China, Hainan, and Taiwan consistently exhibited lower GHI.

EHD exceeded 40 days per summer in Xinjiang and western Gansu and Inner Mongolia, showing persistent spatial patterns. Moderate EHD values (10–30 days) occurred in central and southern BTH, the Shaanxi–Shanxi junction, southern Jiangsu, northern Jiangxi, Hainan, and the Pearl River Delta (e.g., Zhongshan and Dongguan) between 2020 and 2060, and in central and eastern China in 2055–2060.

Correspondingly, PV power losses were highest and spatially stable in Xinjiang, western Qinghai, Gansu, Inner Mongolia, central Ningxia, and central to southern BTH from 2015 to 2060. These losses gradually increased over time. Overall, GHI, EHD, and PV power loss exhibit substantial spatial overlap and remain stable in western China and the central–southern BTH region, where values consistently exceed those in other regions.

Supplementary Note 4. Association of radiation and cell temperature with clouds and aerosols

Clouds and aerosols are major determinants of solar radiation availability and PV panel operating temperatures. Supplementary Fig. 5 shows the interannual variability of summer GHI, TCC, and AOD from 2015 to 2060. GHI exhibits a fluctuating upward trend with a bimodal pattern, peaking around 2030 and 2060 and reaching a minimum near 2035. A strong inverse correlation is observed between GHI and TCC, while the anti-phase relationship between GHI and AOD is weaker—indicating that interannual variability in summer GHI is primarily driven by cloud cover, with aerosols exerting a secondary influence.

To further assess how clouds and aerosols modulate PV performance, we analyzed the interannual variability of PV module cell temperature (Tc) relative to TCC and AOD during extreme heat events (Ta > 35 °C) from 2015 to 2060 (Supplementary Fig. 6). Tc shows a clear inverse phase relationship with TCC across the entire period. Before 2045, Tc and AOD also exhibit an inverse relationship, whereas from 2050 to 2060 both show a concurrent decreasing trend. This pattern suggests that Tc variability is jointly influenced by TCC and AOD until the mid-2040s, after which the influence of aerosols diminishes—likely due to declining aerosol concentrations under strengthened emission controls associated with China's carbon neutrality pathway.

Supplementary Figures

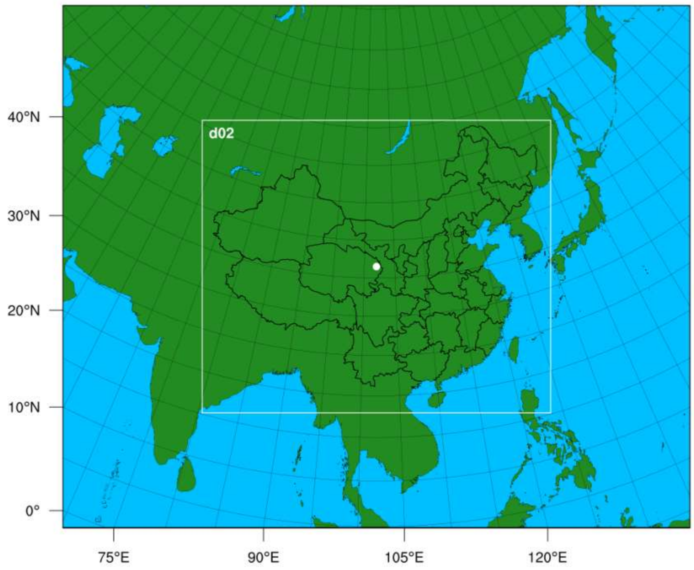

Supplementary Figure 1. Double-nested model domains with horizontal resolutions of 50 km (outer domain) and 10 km (inner domain). The inner domain encompasses China and its surrounding regions.

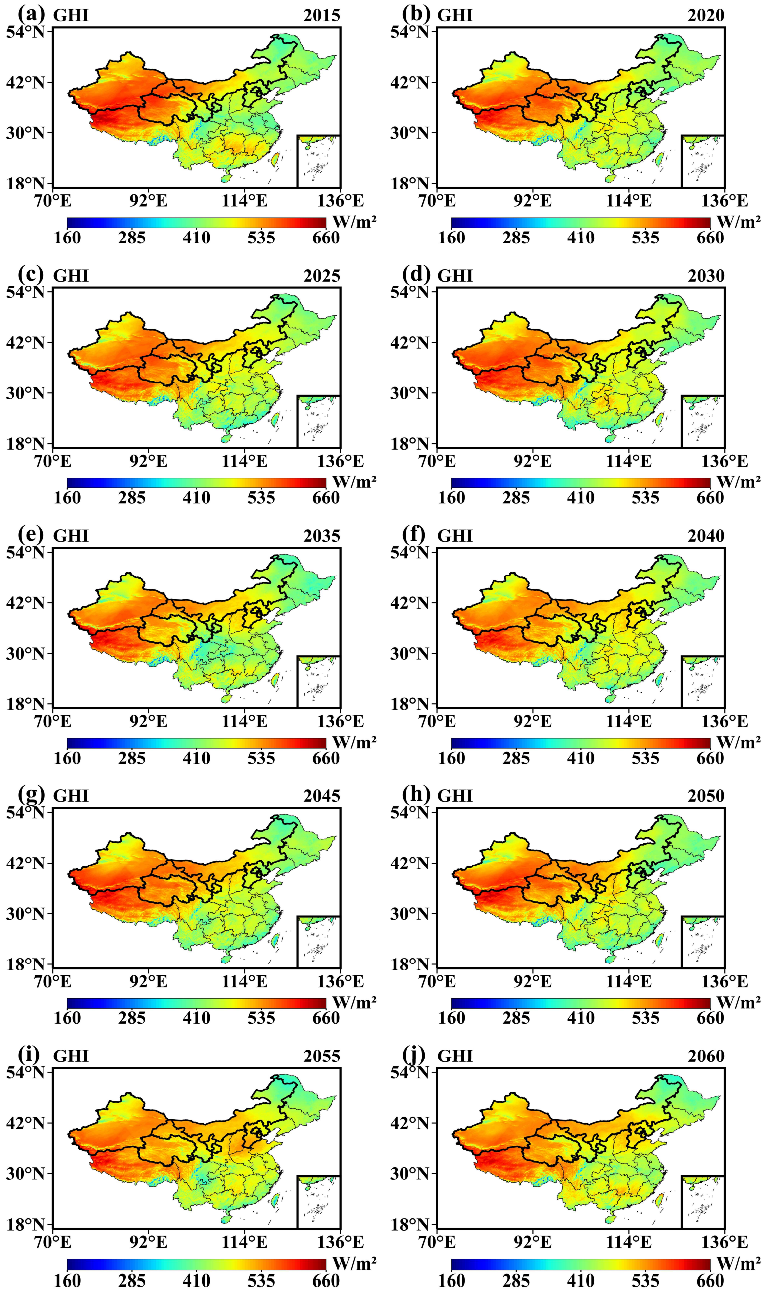

Supplementary Figure 2. Spatial distribution of mean summer global horizontal irradiance (GHI) averaged over 2015–2060. Bold outlines highlight China's major photovoltaic (PV) generation bases—including Xinjiang, Gansu, Inner Mongolia, and Ningxia—or regions with consistently high GHI during 2015–2060, excluding Xizang (Tibet) and western Sichuan where large-scale solar energy development is extremely challenging.

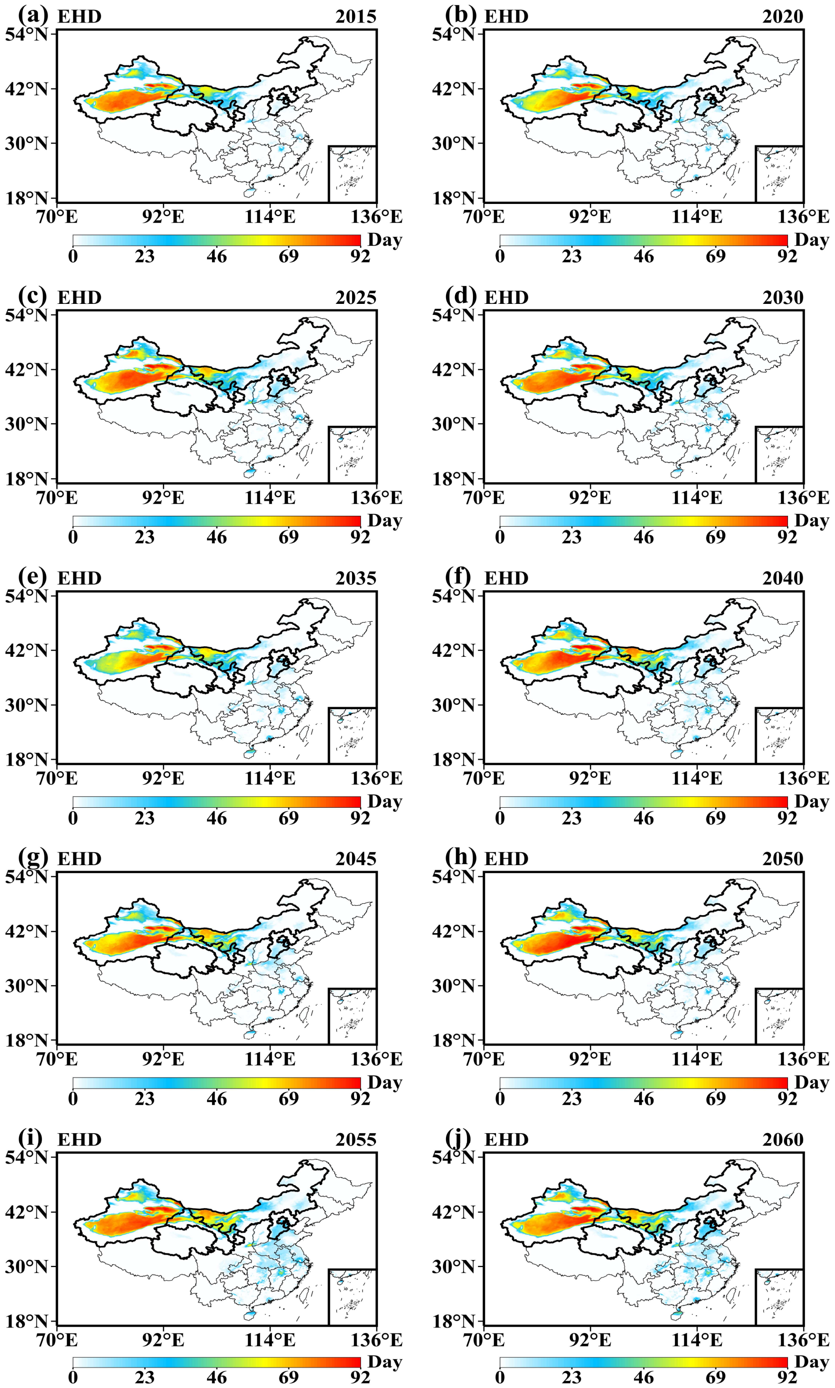

Supplementary Figure 3. Spatial distribution of mean summer extreme hot days (EHD) averaged over 2015–2060. Bold outlines highlight China's major photovoltaic (PV) generation bases, corresponding to regions that experience consistently higher EHD during 2015–2060.

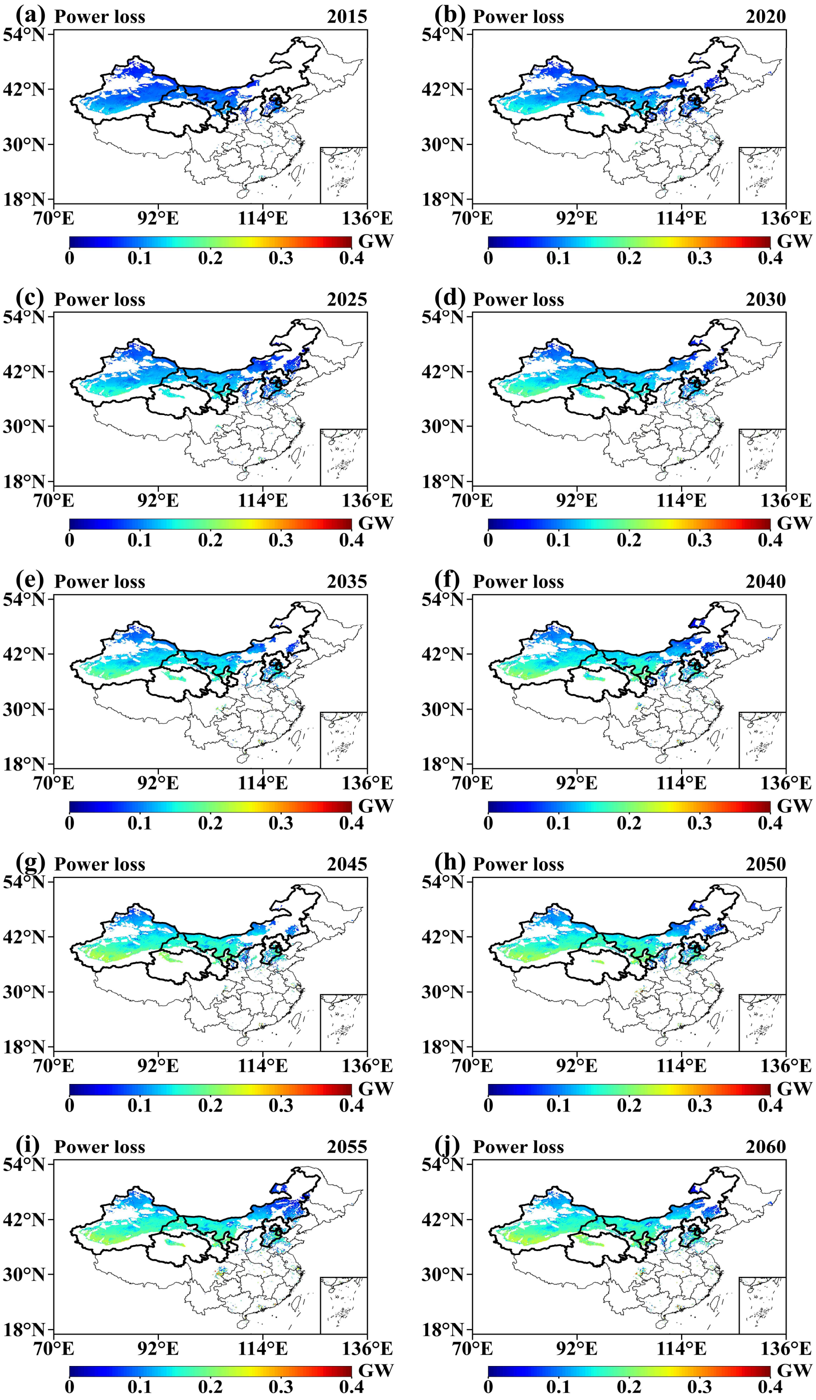

Supplementary Figure 4. Spatial distribution of photovoltaic (PV) power loss during summer averaged over 2015–2060. Bold outlines highlight China's major PV generation bases, corresponding to regions with consistently larger PV power losses over the study period.

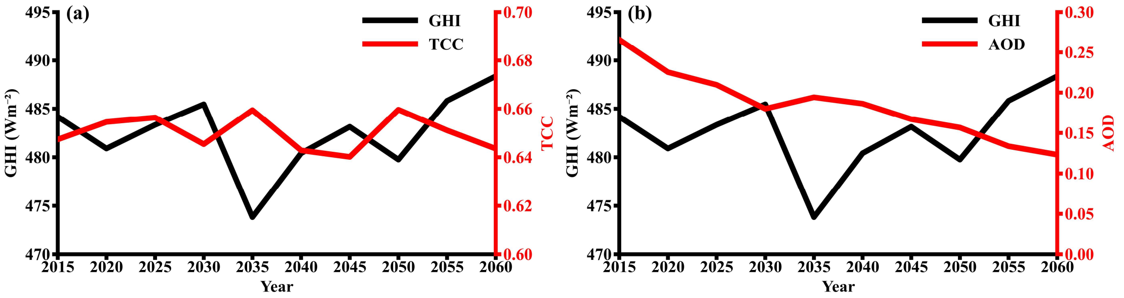

Supplementary Figure 5. Annual variations of mean summer global horizontal irradiance (GHI), total cloud cover (TCC), and aerosol optical depth (AOD) from 2015 to 2060.

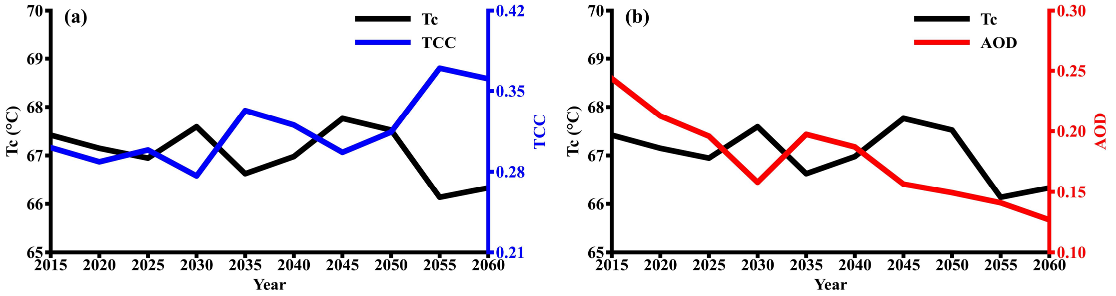

Supplementary Figure 6. Annual variations of mean summer cell temperature (Tc), total cloud cover (TCC), and aerosol optical depth (AOD) during extreme heat events (maximum air temperature, Ta > 35 °C) from 2015 to 2060.

Supplementary Tables

Supplementary Table 1. Input data used in the WRF-Chem model.

Datasets	Socioecnomic scenario	Year of used data	Time interval	Spatial resolution (degree)	Variables or elements
DPEC emission inventory[2]	Ambitious-pollution-Neutral-goal	2015,2020, 2025,2030, 2035,2040, 2045,2050, 2055,2060	One month,	0.25°×0.25°	SO_2, NOx, CO, NMVOC, NH_3, PM_{10}, $PM_{2.5}$, BC, OC, CO_2
Multi-model integrated GCM[3]	SSP2-4.5	every year from 2015-2060	6-hourly	1.25°×1.25°	Sea surface temperature, Sea-level pressure, Surface pressure, Air temperature, Zonal wind, Meridional wind, Relative humidity, Geopotential height, Soil moisture, Soil temperature

Supplementary Table 2. Parameters used in the calculation of PV power and its loss

Constant	Meaning	Value	Unit
$\boldsymbol{\alpha}$	panel albedo	0.1[11]	/
$\mathbf{A}$	suitable land area for PV power generation	0.22 million	km^2
$\boldsymbol{\varepsilon}$	temperature coefficient of PV modules	0.003[12]	℃$^{-1}$
$\boldsymbol{T_{NOCT}}$	nominal operating cell temperature	45[13]	℃
$\boldsymbol{\beta}$	optimum inclination	non-constant varying with latitude[14]	degree
$\boldsymbol{\rho}$	surface albedo	non-constant varying with longitude, latitude and time[15]	/

Supplementary Table 3. Mean photoelectric conversion efficiency at the standard condition (PCE_std) and PV system performance coefficient (K) from 2015 to 2060 proposed by Lu et al.[16]

Year	PCE_std	K
2015	0.160	0.816
2020	0.194	0.831
2025	0.209	0.846
2030	0.224	0.861
2035	0.234	0.871
2040	0.244	0.881
2045	0.254	0.891
2050	0.259	0.896
2055	0.264	0.901
2060	0.269	0.906

Supplementary Table 4. Simulation error of surface solar radiation and air temperature in summer 2015 and 2020. N is the sample number.

	GHI	DNI	DIF	Ta
R	0.77	0.78	0.61	0.92
RMSE	83.02	93.25	25.49	1.65
MB	67.53	68.19	1.15	0.28
NMB	0.16	0.16	0.01	0.01
IOA	0.73	0.78	0.78	0.96
N	520	53	133	14236

Supplementary References

1. Grell, G., Peckham, S., Schmitz, R., et al. Fully coupled “online” chemistry within the WRF model. *Atmospheric Environment* **39**, 6957-6975 (2005).
2. Cheng, J., Tong, D., Zhang, Q., et al. Pathways of China’s PM2.5 air quality 2015–2060 in the context of carbon neutrality. *National Science Review* **8**, nwab078 (2021).
3. Xu, Z., Han, Y., Tam, CY., et al. Bias-corrected CMIP6 global dataset for dynamical downscaling of the historical and future climate (1979–2100). *Scientific Data* **8**, 293 (2021).
4. Emmons, L., Walters, S., Hess, P., et al. Description and evaluation of the Model for Ozone and Related chemical Tracers, version 4 (MOZART-4). *Geoscientific Model Development* **3**, 43-67 (2010).
5. Xu, X., Heng, Z., Li, Y., et al. Improvement of cloud microphysical parameterization and its advantages in simulating precipitation along the Sichuan-Xizang Railway. *Science China Earth Sciences* **67**, 856-873 (2024).
6. Iacono, M., Delamere, J., Mlawer, E., et al. Radiative forcing by long-lived greenhouse gases: calculations with the AER radiative transfer models. *Journal Of Geophysical Research: Atmospheres* **113**, D13103 (2008).
7. Jiménez, P., Dudhia, J., González-Rouco, J., et al. A revised scheme for the WRF surface layer formulation. *Monthly Weather Review* **140**, 898-918 (2012).
8. Grell, G. & Freitas, S. A scale and aerosol aware stochastic convective parameterization for weather and air quality modeling. *Atmospheric Chemistry And Physics* **14**, 5233–5250 (2014).
9. Smirnova, T., Brown, J., Benjamin, S., et al. Parameterization of cold-season processes in the MAPS land surface scheme. *Journal Of Geophysical Research: Atmospheres* **105**, 4077-4086 (2000).
10. Shin, H. & Hong, S. Representation of the subgrid-scale turbulent transport in convective boundary layers at gray-zone resolutions. *Monthly Weather Review* **143**, 250-271(2015).
11. Li, Y., Kalnay, E., Motesharrei, S., et al. Climate model shows large-scale wind and solar farms in the Sahara increase rain and vegetation. *Science* **361**, 1019-1022 (2018).
12. Chen, Z., Cheng, C., Li, F., et al. Short term forecasting methods for solar photovoltaic power. China meteorological industry standard (QX/T 244-2014). 2014, October 24.
13. Akbari M., Mohammadi R., Zamanpour K., et al. Experimental investigation of photovoltaic passive cooling methods using low-cost metallic, ceramic, and cellulose porous media. *Energy Conversion and Management: X* **27**, 101040 (2025).
14. The World Bank Group. The Global Solar Atlas. https://globalsolaratlas.info/support/data-sources.
15. Qu, Y., Liu, Q., Liang, S., et al. Direct-estimation algorithm for mapping daily land-surface broadband albedo from MODIS data. *IEEE Transactions on Geoscience and Remote Sensing* **52**, 907-919(2013).
16. Lu, X., Chen, S., Nielsen, C. P., et al. Combined solar power and storage as cost-competitive and grid-compatible supply for China’s future carbon-neutral electricity system. *Proceedings of the National Academy of Sciences* **118**, e2103471118 (2021).